Proceedings of Japan-France Seminar on Chemical Evolution of Galaxies

Chemical Compositions, Colors, and the Hubble Sequence

Nobuo ARIMOTO
Observatoire de Paris, Section de Meudon,
92190 Meudon, France

Chemical and photometric properties of galaxies with different Hubble type are computed based on an expanded method of evolutionary population synthesis. The comparison of model results with the observed properties reveals that the initial mass function (IMF) is universal ($\mu \cong 1$) for all Hubble types except irregulars and the star formation rate (SFR) per unit mass decreases from ellipticals to irregulars. High SFRs induce a supernovae-driven wind at $t<1$Gyr in ellipticals and at $1\text{Gyr}<t<(T_G-1)$Gyr in S0s, respectively; whereas SFRs are too low to expell the gas from galaxies within a galactic age $T_G=15$Gyr in spirals and irregulars. This well explains why there are two different sequences of galaxies;i.e., a sequence of gas-poor galaxies and that of gas-rich ones.

Keywords: stellar population, chemical evolution, Hubble sequence

1. Introduction

When we study galaxies with different Hubble type, we immediately notice that galaxies are devided into two distinct groups. The first is a group of elliptical and S0 galaxies with little or no gas. Dwarf ellipticals and globular clusters are also classified into this group. All these spheroidal systems seem to belong to a single family of their masses. The second group consists of spiral and irregular galaxies which still hold a lot of gas and young populations. On an average, early spirals are more luminous than late spirals, and late spirals than irregulars. Therefore, there also seems to be a certain correlation between mass and the Hubble type of gas-rich galaxies,[1] although it is pointed out that the mass range of all Hubble types earlier than Sd overlaps each other.[2]

We wish to know why galaxies with different mass split into gas-poor and gas-rich sequences. Concerning the Hubble sequence, other fundamental facts of observation are as follows;[2] (1) galaxies in the gas-poor sequence have larger bulge-to-disk ratio than those in the gas-rich sequence, and among gas-rich galaxies, the bulge-to-disk ratios of early spirals are larger than those of late spirals and irregulars. (2) At a fixed luminosity, the gas-poor galaxies have redder integrated colors than the gas-rich ones. Especially, a separation of the gas-poor and the gas-rich sequences is well defined in the (U-V,V-K) diagram (Fig.6). (3) There is a trend that the hydrogen mass-to-luminosity ratio increases from early spirals to irregulars. These facts should also be explained by

the scenario which identifies the reason why two different sequences are formed.

As is shown in Fig.6, the integrated colors of galaxies are closely correlated with their Hubble types. Since the integrated colors are sensitive to the population structure of stars with different mass, age, and chemical composition, only a particular history of star formation reproduces the observed photometric properties of a galaxy. Therefore, with the specified SFR and the IMF, it is possible to synthesize the stellar populations of galaxies which belong to a certain morphological type.

2. Expanded Evolutionary Method

The method of evolutionary population synthesis has been applied to analyses of the integrated lights of various galaxies.[3),4),5)] In constructing population models, earlier works were restricted mostly to the ideal situation where stars always evolve along the tracks with solar abundance in the HR diagram. According to chemical evolution, however, the frequency distribution of stellar metallicities is determined by how much mass of a galaxy has turned into stars with a certain mass spectrum. Since the metallicity of the gas from which stars are formed is an important parameter of stellar evolutionary tracks, an approximation of constant metallicity is inappropriate to study the photometric evolution of galaxies.

Arimoto and Yoshii[6)] developed the so-called expanded evolutionary method for the photometric evolution of a galaxy, taking into account the fact that the metallicity of newly formed stars should change as a galaxy evolves (hereafter AY models). AY models assume that a galaxy is a closed system and the gas is always well-mixed and distributed uniformly. Then under the adopted forms of the IMF $\phi(m)$ and the SFR $C(t)$, the full set of equations for the chemical evolution is integrated without instantaneous recycling approximation. A power-law form is assumed for the IMF, $\phi(m) \propto m^{-\mu}$, in the mass range $0.05 \leq m/m_{\odot} \leq 60$ ($\mu=1.35$ for the local Salpeter IMF). The SFR proportional to the fractional gas mass is assumed, $C(t)=\nu f_g(t)$, where ν is normalized by a value $\nu_{\odot}=6.08\ 10^{-18}\ \mathrm{sec}^{-1}$ which corresponds to the SFR per unit mass in the solar neighbourhood provided that $T_G=15\mathrm{Gyr}$ for our Galaxy.

To incorporate explicitly the effects of stellar metallicity on the photometric properties of a galaxy, the change in luminosity and effective temperature of stars born with different metallicities are followed by using appropriate evolutionary tracks. The blanketing correction due to the metallic lines in stellar atmosphere is also taken into account by using empirical and theoretical photometirc calibrations. Thus, AY models are applicable to galaxies composed of stars with various abundances of metallicity. For the details of AY models the reader should consult the original paper.[6)]

3. Gas-poor Sequence

3.1 Giant Elliptical Galaxies

Elliptical galaxies are believed to have undergone active star formation in

the initial stage of evolution. Since a higher rate of star formation naturally brings about a higher rate of supernovae explosions, a supernovae-driven galactic wind would occur preferentially in elliptical galaxies.[7),8)]

Introducing a galactic wind into the AY models, Arimoto and Yoshii[9)] compute chemical and photometric properties of elliptical galaxies. The authors assume that a galaxy is supported against collapse by supersonic motion of interstellar clouds and that star formation is induced by cloud collisions. The chemical evolution is traced until a wind is induced at t_{GW} when the thermal energy of the gas heated up by supernovae explosions exceeds the binding energy of the gas.[7)]

Let the initial mass of a galaxy be $M_G=10^{12}M_\odot$, then the coefficient ν, from which t_{GW} is evaluated, is so obtained as to give $M_V\cong-23$ mag at the present age $T_G=15$Gyr. As a result, $\nu/\nu_o\cong50$ and $t_{GW}\cong1$Gyr are obtained, provided $\mu=1.35$. Figure 1 shows the Johnson's (1966) broad-band colors of the composite population models as a function of μ. Contrary to the widely accepted result based on single burst population models, the synthesized UBVRIJKL colors show strong dependency on the stellar metallicity and hence on the slope of the IMF. The model with $\mu\cong1$ gives an excellent fit to the observations simultaneously from U-B to V-K. Thus, it is concluded that the IMF of giant ellipticals is characterixed by the slope of $\mu\cong1$.

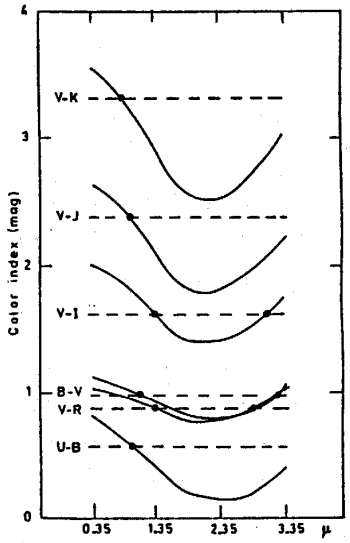

Fig.1

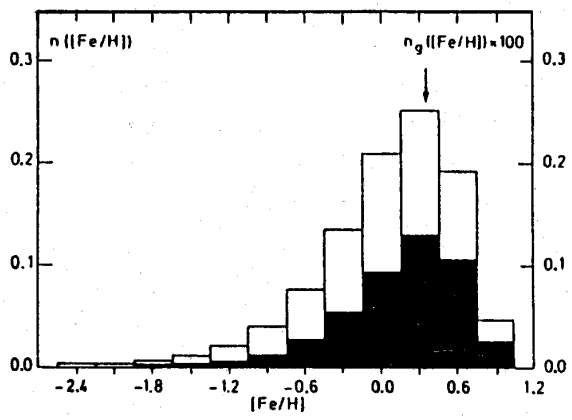

Fig.2

Fig.1 Integrated colors of the models plotted against the power index μ of the IMF. The curves represent loci of models with varying μ and constant ν/ν_o (=50). Dashed-lines are the empirical values of an average giant elliptical(24).

Fig.2 Metallicity distribution of stars in the model of $M_G=10^{12}M_\odot$. Model parameters are $T_G=15$Gyr, $\mu=0.95$, $\nu/\nu_o=50$, and $t_{GW}=1$Gyr. The open and filled columns represent number fractions of total stellar populations n and giant n_g, respectively. The arrow indicates the average stellar metallicity weighted by luminosity.

The metallicity distribution for the stellar populations in a model giant elliptical with $\mu=0.95$ is represented in Fig.2. It appears that a giant elliptical is the true composite stellar system where stellar metallicities range from [Fe/H] =-2.4 to +0.9. It must be noted that this metallicity range remarkably

resembles to that determined for giants in the nuclear bulge of our Galaxy.[10]

3.2 Color-Magnitude Relation

It has been emphasized that the integrated colors of ellipticals become progressively bluer as the luminosity decreases. Arimoto and Yoshii[9] compute the models of $M_G=10^9$-$2\ 10^{12}M_\odot$ with T_G=15Gyr, μ=0.95, and $\nu/\nu_o=45(M_G/10^{12}M_\odot)^{-0.1}$ A dependency of ν on M_G is derived by assuming that a time scale of star formation is equal to that of cloud collisions and that proto-ellipticals had obeyed the same mass-radius relation as presently observed for globular clusters and ellipticals.[13]

The wind models give a relation $\log(t_{GW}/\mathrm{Gyr})=0.44\ \log(M_G/10^9M_\odot)-1.46$, which indicates that a galactic wind occurs later and star formation continues much longer in larger galaxy, because the binding energy of a galaxy per unit mass increases with an increase of M_G. It is interesting to point out that even for the most massive case a wind occurs earlier than the collapse time $t_c\cong$1Gyr. Thus no disk forms in elliptical galaxies.

The final metallicity $Z_g(t_{GW})$ of the gas increases rapidly according to a relation $Z_g(t_{GW})=y\ln f_g(t_{GW})^{-g_1}$ as M_G increases, where $y\cong0.06$ is a yield value for μ=0.95. The model predicts that each of elliptical with $M_G\geq10^{11}M_\odot$ releases an amount of $10^9M_\odot$ heavy elements in a wind. This may explain the origin of iron-enriched gas in intracluster space.

The frequency distribution of metallicity in each model is similar to Fig.2, but the maximum frequency occurs at lower value of [Fe/H] for smaller M_G. In the case of less massive galaxy, the distribution is truncated at higher metallicity, because the chemical evolution is stopped by a wind before it is completed.

The average of stellar metallicity weighted bu luminosity is defined as

$$<[\mathrm{Fe/H}]>=\Sigma_{i,j}n_{ij}[\mathrm{Fe/H}]_iL_j/\Sigma_{i,j}n_{ij}L_j,$$

where n_{ij} is the number of stars binned into the intervals centered on $[\mathrm{Fe/H}]_i$ and $\log L_j$. Then the models show that the average stellar metallicity increases from $<[\mathrm{Fe/H}]>=-0.74$ to +0.33, as the absolute magnitude decreases from $M_V=-14$ to -24 mag. The metallicity-mass relation is approximated such that $Z\propto M^{0.45}$ for $M<10^{10}M_\odot$ and $Z\propto M^{0.15}$ for $M\geq10^{10}M_\odot$. The prediction agrees well with the empirical relation, $Z\propto M^{0.4}$, given by Mould[15] for dwarf spheroidals and giant ellipticals.

Figure 3 shows the integrated colors at T_G=15Gyr as a function of M_G. All the integrated colors become redder with increasing M_G. This monotonic reddening of the color is closely related to the monotonic increase in $<[\mathrm{Fe/H}]>$. Since the (V-K) color is free from uncertainties due to blanketing of individual stars and contamination by young stars, it geneinely represents the metallicity of late giants in a galaxy. Moreover, as shown in Fig.3, the color difference for a fixed range of metallicity is largest in (V-K), thus (V-K) can be used as an excellent metallicity indicator of elliptical galaxies. The best linear fit to the model results is $V-K=3.07+0.71[\mathrm{Fe/H}]$.

Figure 4 represents color-magnitude diagrams in various wavelengths. The

agreement between the empirical and modal CM relations is satisfactory from the ultraviolet to infrared colors. Slight discrepancies in (U-V) and (V-K) may be attributed to neglections of metal-poor HB stars and SMR giants which contribute to the ultraviolet and infrared colors, respectively. Thus, it is concluded that a supernovae-driven wind model accounts for the observed trend of the CM relation that the colors of elliptical galaxies become redder for higher luminosity.

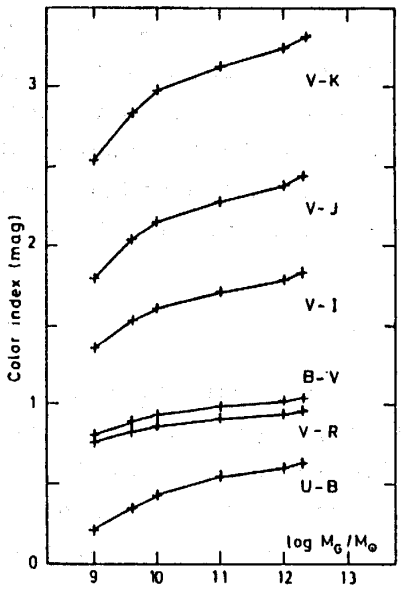

Fig.3

Fig.3 Integrated colors of the models at 15Gyr against the initial mass M_G of a galaxy.

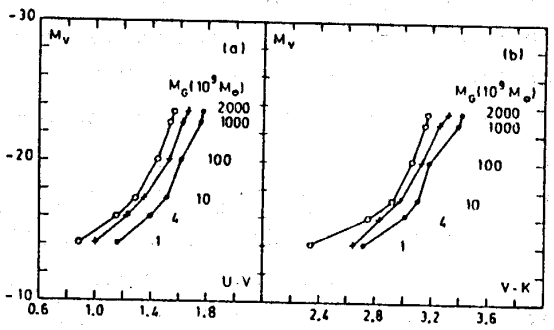

Fig.5

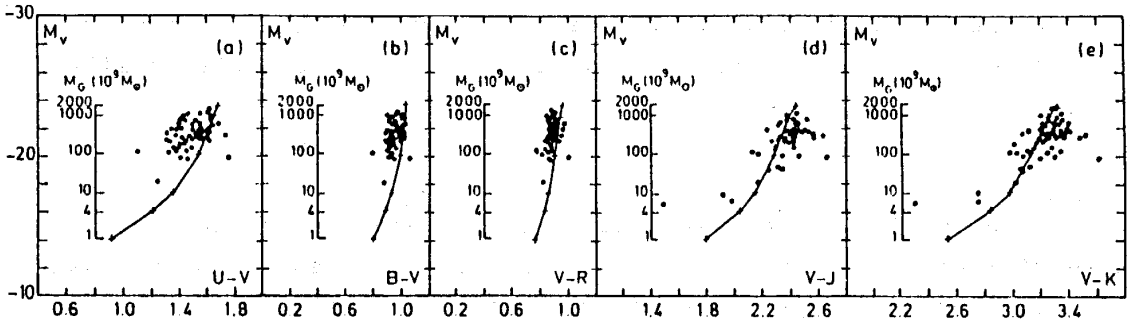

Fig.4

Fig.4 CM relations predicted by the composite models. The numerical values denote initial mass M_G of a galaxy in units of $10^9 M_\odot$. The filled circles give the observational data of ellipticals in field, Virgo and Coma clusters (17).

Fig.5 Effects of the SFR on the CM relations. The crosses represent the standard CM relation. The filled and open circles represent the CM relations predicted by the models with the lower ($\nu/\nu_0 = 25(M_G/10^{12}M_\odot)^{-0.1}$) and higher ($\nu/\nu_0 = 65(M_G/10^{12}M_\odot)^{-0.1}$) SFRs, respectively.

3.3 Intrinsic Dispersion in the CM Relation

There is considerable scatter around the empirical CM relation (Fig.4).

The width of scatter is greater than observational error and seems to be intrinsic. Pickles[16] suggested that variations in the number of recently formed stars could account for the scatter around the CM relation in the (M_V,U-V) diagram. However, from data by Persson et al.,[17] we have found that there is a tight correlation between the color excess from the average CM relation in (U-V) and that in (V-K);i.e., at a fixed magnitude, ellipticals redder in (U-V) are also redder in (V-K). Thus, it is unlikely that young stars are the cause of these scatters, because the (V-K) color is free from contamination by young stars.[6] Instead, we suggest that an intrinsic dispersion in the SFR at a fixed M_G could explain this scatter. At a fixed value of M_G, a lower SFR reduces the rate of supernovae explosions, which induces a wind much later. As a result, the average stellar metallicity increases and the integrated colors shift redward, whereas the absolute magnitude remains nearly constant. The predicted widths of scatter around the CM relation in the (M_V,U-V) and (M_V,V-K) diagrams are shown in Fig.5, which agree satisfactorily with the observed ones.

3.4 Dwarf Ellipticals and Globular Clusters

Applying the wind model to much smaller systems of dwarf ellipticals and globular clusters, Yoshii and Arimoto[18] successfully reproduce the structural and chemical properties of ellipticals, dwarf ellipticals, and metal-poor globular clusters. The chemical and photometric properties of the spheroidal systems lie on the monotonical relations with their masses (As an example of the results, the modal sequence in the (U-V,V-K) diagram is shown in Fig.6). Whereas, the expansion of a system due to galactic mass loss changes the structural properties mostsignificantly for dwarf ellipticals, which explains well the distinct distributions of spheroidal systems in the diameter-surface brightness diagram.[19] Hence, it is concluded that all spheroidal systems are a one parameter family of mass at their birth.

3.5 S0 Galaxies

As shown in Fig.6, the distribution of S0 galaxies in the (U-V,V-K) diagram is quite similar to that of elliptical galaxies. This suggests that galaxies of both Hubble types had experienced nearly the same history of star formation, especially the same IMF. On the other hand, S0s have disks and HI gas is preferentially detected in S0s, which implies at least that the star formation continued longer in S0s than ellipticals. In Sect.3.3 we saw that at a fixed M_G a wind is induced later if the SFR is smaller. This suggests that, if we adopt a slightly smaller value of ν/ν_o for S0s than that for ellipticlas, star formation continues longer enough to form a disk and eventually a wind expells the gas.

Computing a series of models with $M_G=10^{12}M_\odot$, T_G=15Gyr, μ=0.95, ν/ν_o=32, and varying t_{GW}, we find that the resulting colors are consistent with the observed S0s so far as t_{GW} is less than (T_G-1)Gyr (It should be noted that the S0 models are preliminary ones, because t_{GW} is treated independently of M_G, although certain correlations should be exist as is the case for ellipticals). In Fig.6, the

distribution of the S0 models is also shown.

As a result of longer continuation of chemical evolution, the average stellar metallicity of S0s is $[Fe/H]=0.23$ which is slightly higher than $[Fe/H]=0.26$ of ellipticals with the same M_G.

Since disk stars in S0s are younger and more massive than stars in ellipticals, a higher accumulation rate of the gas ejected from evolved stars is expected after a galactic mass loss. If the star formation continues longer, then the average mass of disk stars becomes larger and a higher value of HI gas will be detected. This suggests that the de Vaucouleurs numerical sequence of S0 subtypes -3, -2, and -1 is a sequence of S0s with increasing t_{GW}, because the observed HI content increases significantly along this sequence.[20)]

4. Gas-Rich Sequence

4.1 Early and Late Type Spiral Galaxies

Discussions in Sects.3.3 and 3.5 suggest that the SFRs for galaxies in the gas-rich sequence should be smaller than that for S0 galaxies; otherwise the explosion rate of supernovae is high enough to transmute galaxies into the gas-rich sequence. In Fig.6, we illustrate loci of AY models[6)] computed for a grid of $(\nu/\nu_o,\mu)$;i.e., $M_G=10^{12}M_\odot$, $T_G=15$Gyr, $\nu/\nu_o=0.01$-10, and $\mu=0.35$, 1.35, and 2.35. As extensively discussed in Arimoto and Yoshii,[6)] the integrated colors of the composite models are quite sensitive to a history of star formation, especially to the choices of ν/ν_o and μ. The very young stars mainly contribute to the (U-V) color, whereas the average stellar metallicity is essential to the (V-K) color. Since both the relative number of young stars and the average metallicity are strong functions of ν/ν_o and μ, each locus of models with varying ν/ν_o and constant μ completely separates from each other.

One cannot know *a priori* what kind of the IMF is appropriate for galaxies in the gas-rich sequence, but Fig.6 strongly demonstrates that the Salpeter-like IMF with a certain value of μ between 0.35 and 1.35 would be the most plausible one. Thus, we newly compute an additional sequence of models with $M_G=10^{12}M_\odot$, $T_G=15$Gyr, $\nu/\nu_o=0.01$, 0.1, 1, 2, 4, 8, 16, and $\mu=0.95$. The resulting locus of models with decreasing ν/ν_o from 16 to 0.01 reproduces satisfactorily the continuous change of observed colors from early spirals to late spirals, and then to irregulars (Fig.6).

One of the observed quantities characteristic to gas-rich galaxies is the hydrogen mass-to-luminosity ratio. Figure 7 shows the $(\log M_H/L_B, U-V)$ diagram. It appears that the model also explain well such a monotonic increase of $\log M_H/L_B$ from early spirals to late ones.

The average stellar metallicities predicted for early and late spirals are nearly constant ($[Fe/H]=0.57$) and are slightly higher than those for ellipticals and S0s. Rich[12)] has recently found many SMR giants with $[Fe/H]<0.5$ in the nuclear bulge of our Galaxy. The infrared photometry reveals that brighter spirals with the absolute H magnitude $H^{abs}<-21$ mag have redder (J-K) colors than ellipticals and S0s of the same magnitude.[21)] Since (J-K) is a good indicator of the average

metallicity, the infrared photometry seems to support the present prediction.

As a conclusion, spiral galaxies have the same IMF as ellipticals and S0s and the SFR per unit mass decreases from early to late spirals.

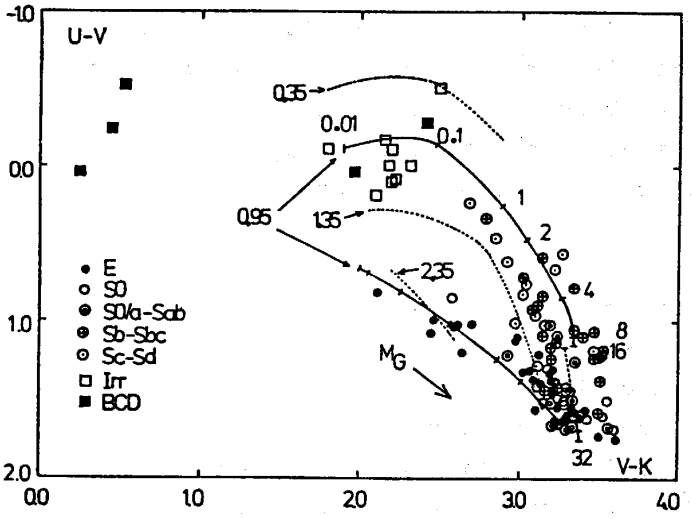

Fig.6

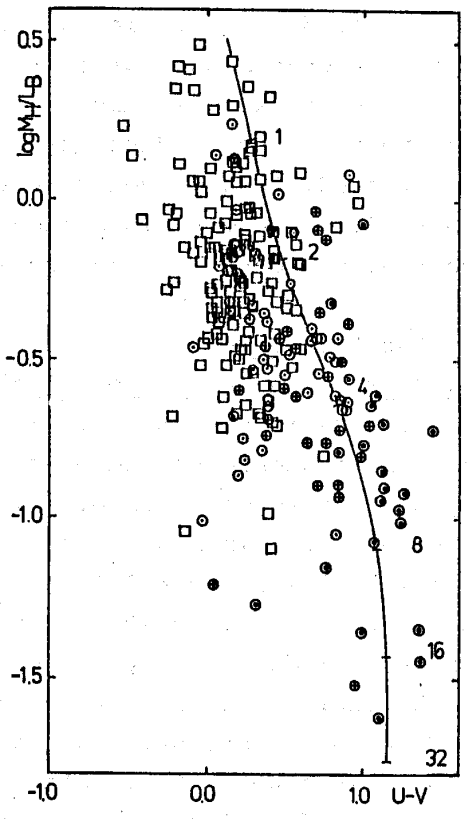

Fig.7

Fig.6 Gas-poor and gas-rich sequences in the (U-V,V-K) diagram. For a gas-poor sequence, models are computed with T_G=15Gyr, μ=0.95, $M_G=10^6$-$2\ 10^{12}M_\odot$, and $\nu/\nu_o=45(M_G/10^{12}M_\odot)^{-0.1}$ for $M_G \geq 10^8M_\odot$ and $=200(M_G/10^8M_\odot)^{-0.3}$ for $M_G<10^8M_\odot$. For a gas-rich sequence, with T_G=15Gyr, μ=0.95, $M_G=10^{12}M_\odot$, and ν/ν_o=0.01-16 (solid locus) and with T_G=15Gyr, μ=0.35, 1.35, 2.35, $M_G=10^{12}M_\odot$, ν/ν_o=0.01-10 (dotted loci). Models for S0s are with T_G=15 Gyr, μ=0.95, $M_G=10^{12}M_\odot$, ν/ν_o=32, and t_{GW}=1-14Gyr. Observational data are taken from literature (17,25,29,31).

Fig.7 The ($\log M_H/L_B$,U-V) diagram for a gas-rich sequence. Models are computed with T_G=15Gyr, μ=0.95, $M_G=10^{12}M_\odot$, and ν/ν_o=0.01-16. Observational data are taken fromliterature (26,27,29,32,33).

4.2 Irregular Galaxies

Figure 6 shows that the observed colors of irregular galaxies are consistent with models having ν/ν_o=0.01-0.1 and μ=0.95. The abundance of heavy elements of the gas given by these models is in the range of $-1.2 \lesssim \log Z_g/Z_\odot \lesssim -0.2$, which also agrees well with the observed ones.[22] However, Fig.7 indicates a significant discrepancy that the models give much higher values of $\log M_H/L_B$ than the observed irregulars; that is, irregulars show too low fractionary gas mass for their estimated metal abundances. This suggests that some particular history of star formation is required to understand both chemical and photometric properties of

irregulars.

One of ways out of this difficulty is to suppose that the chemical evolution of small galaxies is directly controlled by local IMFs of individual sites of star formation, in contrast to large galaxies where the chemical evolution is described by the overall and time-constant IMF defined as an ensemble of local IMFs. In such a case, photometric properties of irregulars are mainly determined by several regions presently active and their chemical properties are given as the integrated results of past star formations. To reproduce the observed blue colors of irregulars, the slope of the IMF must be $\mu \cong 1$, as shown in Fig.6, whereas the observed abundance of heavy elements and fractionary gas mass require a more steep IMF with $\mu \cong 2$. This suggests that the past star formations were characterized by the steep IMF but the present day star formations are by the flat IMF. Thus, the IMF is not time-constant in an irregular galaxy and an average slope of the IMFs of individual sites might decrease as evolution proceeds.

5. Discussions

Previous sections indicate that the properties of galaxies are well explained if the SFRs decrease along the Hubble sequence from ellipticals to late spirals. The high SFRs induce a wind in ellipticals within the collapse time of a galaxy and in S0s after the formation of disks. Whereas the decreasing SFRs, which are too low to induce a wind within the Hubble time, devide gas-rich galaxies into the Sa, Sb, Sc, Sd, and Sm types with the decreasing bulge-to-disk ratio and the increasing abundance of gas and young stars.

Let's consider why the SFRs decrease from early to late type galaxies. It is noticed that forms of ellipticals are essentially supported by random motion of stars, whereas gas and stars in irregulars rotate almost regidly. These facts suggest that the random component decreases monotonically with respect to the rotational motions from early to late type galaxies. In ellipticals, the random motion is so dominant that the frequency of cloud collisions, and hence the SFRs during the stage of bulge formation is extreamly high. From early to late types, the rotational motion becomes prominent, which surpresses the cloud collisions and gives smaller SFRs during bulge formation. As a result, the SFR in the bulge is a function of Hubble type.

As for the SFR in the disk, since a density wave developes well in the disk of a sufficiently large spiral rotating differentially, stars are mainly formed in the regions compressed by the shocks. Then, the SFR could be given as

$$\nu/\nu_o \propto k(\Omega-\Omega_p),$$

where k is the number of arms, Ω the angular velocity of material in circular orbit, and Ω_p the pattern speed.[28] Since the maximum velocity of a spiral galaxy along its rotation curve decreases gradually from early to late spirals[23], the SFRs during disk formation would be smaller in late spirals than early ones. Especially in irregulars which rotate rigidly because of their small sizes, there is no growth of density wave. Stars are formed locally and stocastically. Thus, the star formation in irregulars is less efficient with respect to late spirals.

Above discussions indicate that the SFRs during both bulge and disk formations decrease from ellipticals to irregulars. If mass of a galaxy is constant independent of its morphology, it could be said that the Hubble sequence is a sequence of galaxies with decreasing angular momentum. However, a galactic mass actually tends to decrease from early to late types. Therefore, a certain correlation between a mass and an angular momentum of a galaxy could have been an initial condition for galaxy formation.

6. Conclusion

By using the expanded evolutionary method of population synthesis, we compute the chemical and photometric properties of galaxies with different Hubble type.

The comparison of model results with the observed properties reveals: (1) the IMF is universal ($\mu \cong 1$) for all Hubble types except irregular for which the IMF cannot be defined statistically because of their small sizes. (2) The star formation rate per unit mass decreases from ellipticals to irregulars. (3) The spheroidal systems such as giant and dwarf ellipticals and globular clusters are the one parameter family of mass at their birth. (4) The high SFRs induce a supernovae-driven wind at $t<1$Gyr in ellipticals and at $1\text{Gyr}<t<(T_G-1)$Gyr in S0s, respectively; whereas the SFRs are too low to expell the gas from galaxies within a galactic age $T_G=15$Gyr in spirals and irregulars. This well explains why there are gas-poor and gas-rich sequences of galaxies. (5) The average stellar metallicities of spirals are slightly higher than those of ellipticals and S0s of the same magnitude. (6) Some particular history of star formation is required to understand both the chemical and photometric properties of irregular galaxies.

Acknowlegements: We thank I.Tarrab, C.Balkowski, A.Pickles, R.Cayrel, K.Kodaira, and Y.Yoshii for discussions. We particularly thank G.Cayrel de Strobel, J.C.Pecker, and K.Kodaira who arranged his stay in Observatoire de Paris-Meudon. The computations were mainly carried out on a VAX 11/780 at Observatoire de Paris-Meudon. This work was supported in part by Scientific Research Funds of Ministry of Education, Science, and Culture of Japan (No.60740129), and in part by the Laboratoire Associe 335 of the Conseil National de la Recherche Scientifique of France.

References

1) Tully,R.B.,Mould,J.R.,Aaronson,M.: 1982, Astrophys.J. 257, 527.
2) Sandage,A.: 1986, Astron.Astrophys. 161, 89.
3) Tinsley,B.M.: 1972, Astron.Astrophys. 20, 383.
4) Tinsley,B.M.: 1980, Fund.Cosmic Physics 5, 287.
5) Bruzual,A.G.: 1983, Astrophys.J. 273, 105.
6) Arimoto,N.,Yoshii,Y.: 1986, Astron.Astrphys. 164, 260.
7) Larson,R.B.: 1974, Monthly Notices Roy.Astron.Soc. 169, 229.
8) Ikeuchi,S.: 1977, Prog.Theor.Phys. 58, 1742.

9) Arimoto,N.,Yoshii,Y.: 1987, Astron.Astrophys. 173, 23.
10) Whitford,A.E.,Rich.R.M.:1983, Astrophys.J.274, 723.
11) Whitford,A.E.: 1985, Publ.Astron.Soc.Pacific 97, 589.
12) Rich,R.M.: 1986, private communication.
13) Saito,M.: 1979, Publ.Astron.Soc.Japan. 31, 181.
14) Yoshii,Y.,Saio,H.: 1985, Astrophys.J. 295, 521.
15) Mould,J.R.: 1984, Publ.Astron.Soc.Pacific 96, 773.
16) Pickles,A.J.: 1985, Astrophys.J. 296, 340.
17) Persson,S.E.,Frogel,J.A.,Aaronson,M.: 1979, Astrophys.J.Suppl. 39, 61.
18) Yoshii,Y.,Arimoto,N.: 1987, Astron.Astrophys. submitted.
19) Ichikawa,S., Wakamatsu,K.,Okamura,S.: 1986, Astrophys.J.Suppl. 60, 475.
20) Chamaraux,P.,Balkowski,C.,Fontanelli,P.: 1986, Astron.Astrophys. 165, 15.
21) Bothun,G.D.,Aaronson,M.,Schommer,B.,Mould,J.,Huchra,J.,Sullivan,W.T.III: 1985, Astrophys.J.Suppl. 57, 423.
22) Gallagher,J.S.III,Hunter,D.A.: 1984, Ann.Rev.Astron.Astrophys. 22, 37.
23) Giraud,E.: 1984, Ph.D.thesis, University of Montpellier, France.
24) Tinsley,B.M.: 1978, Astrophys.J. 224, 14.
25) Aaronson,M.: 1978, Astrophys.J.Letters 221, L103,
26) Hunter,D.,Gallagher,J.,Rautenkranz,D.: 1982, Astrophys.J.Suppl. 49, 53.
27) Bothun,G.D.,Aaronson,M.Scommer,B.,Mould,J.,Huchra,J.,Sullivan,W.T.III.: 1985, Astrophys.J.Suppl. 57, 423.
28) Talbot,R.J.,Arnett,W.D.: 1975, Astrophys.J. 197, 551.
29) Thuan,T.X.: 1983, Astrophys.J. 268, 667.
30) Thuan,T.X.,Martin,G.E.: 1981, Astrophys.J. 247, 823.
31) Hunter,D.A.,Gallagher,J.S.III: 1985, Astron.J. 90, 1457.
32) de Vaucouleurs,G.,de Vaucouleurs,A.,Buta,R.: 1981, Astron.J. 86, 1429.
33) de Vaucouleurs,G.,de Vaucouleurs,A.,Buta,R.: 1983, Astron.J. 88, 764.